REPORT

# Mutations in *CAPN1* Cause Autosomal-Recessive Hereditary Spastic Paraplegia

Ziv Gan-Or,[1,2,3,15] Naima Bouslam,[4,15] Nazha Birouk,[5,15] Alexandra Lissouba,[6,7,15] Daniel B. Chambers,[8] Julie Vériepe,[6,7] Alaura Androschuck,[8] Sandra B. Laurent,[1,3] Daniel Rochefort,[1,3] Dan Spiegelman,[1,3] Alexandre Dionne-Laporte,[1,3] Anna Szuto,[1] Meijiang Liao,[6,7] Denise A. Figlewicz,[10] Ahmed Bouhouche,[4] Ali Benomar,[4] Mohamed Yahyaoui,[4] Reda Ouazzani,[5] Grace Yoon,[11,12] Nicolas Dupré,[13] Oksana Suchowersky,[14] Francois V. Bolduc,[8] J. Alex Parker,[6,9] Patrick A. Dion,[1,3] Pierre Drapeau,[6,7] Guy A. Rouleau,[1,2,3,*] and Bouchra Ouled Amar Bencheikh[1,6]

Hereditary spastic paraplegia (HSP) is a genetically and clinically heterogeneous disease characterized by spasticity and weakness of the lower limbs with or without additional neurological symptoms. Although more than 70 genes and genetic loci have been implicated in HSP, many families remain genetically undiagnosed, suggesting that other genetic causes of HSP are still to be identified. HSP can be inherited in an autosomal-dominant, autosomal-recessive, or X-linked manner. In the current study, we performed whole-exome sequencing to analyze a total of nine affected individuals in three families with autosomal-recessive HSP. Rare homozygous and compound-heterozygous nonsense, missense, frameshift, and splice-site mutations in *CAPN1* were identified in all affected individuals, and sequencing in additional family members confirmed the segregation of these mutations with the disease (spastic paraplegia 76 [SPG76]). *CAPN1* encodes calpain 1, a protease that is widely present in the CNS. Calpain 1 is involved in synaptic plasticity, synaptic restructuring, and axon maturation and maintenance. Three models of calpain 1 deficiency were further studied. In *Caenorhabditis elegans*, loss of calpain 1 function resulted in neuronal and axonal dysfunction and degeneration. Similarly, loss-of-function of the *Drosophila melanogaster* ortholog calpain B caused locomotor defects and axonal anomalies. Knockdown of *calpain 1a*, a *CAPN1* ortholog in *Danio rerio*, resulted in abnormal branchiomotor neuron migration and disorganized acetylated-tubulin axonal networks in the brain. The identification of mutations in *CAPN1* in HSP expands our understanding of the disease causes and potential mechanisms.

Hereditary spastic paraplegia (HSP) includes a rare group of neurological disorders with an estimated prevalence of 2–10/100,000 individuals in different populations.[1–3] HSP can be classified as pure or complicated on the basis of the clinical presentation. Pure HSP is characterized by progressive spasticity and weakness, limited to the lower limbs, and often manifests as deep-tendon hyperreflexia and the extensor plantar response. Additional often-reported features of the pure form are a hypertonic bladder and lower-limb sensory disturbances. Complicated HSP is accompanied by other neurological symptoms, including seizures, ataxia, intellectual disability, dementia, extrapyramidal symptoms, peripheral neuropathy (if other causes of peripheral neuropathy are ruled out), amyotrophy, optic atrophy, and others.[3,4] Although HSP can be debilitating, individuals with HSP often have a normal lifespan; therefore, post-mortem studies are not common, and neuropathological data are limited. However, the available information indicates that HSP is typically characterized by axonal degeneration of the descending corticospinal tract and ascending sensory fibers.[5] HSP is a genetically heterogeneous disease; currently, there are more than 70 known or suspected genes or genetic loci in which mutations have been suggested to cause HSP.[6,7] Some of the genes are exclusively associated with pure or complicated HSP; however, other genes are associated with both forms of HSP, indicating that other genetic or environmental factors can modify the disease course. HSP can be inherited in an autosomal-dominant (AD-HSP [MIM: 182601]), autosomal-recessive (AR-HSP [MIM: 604360]), or X-linked (XL-HSP) manner. Mutations in *SPAST* (MIM: 604277) account for about 40% of AD-HSP,[8] and homozygous or compound-heterozygous mutations in *SPG11* (MIM: 610844) are the most common cause of AR-HSP.[4] Both genes are thought to be involved in endosomal trafficking, and other HSP-related genes are involved in different pathways, such as mitochondrial regulation, lipid metabolism, and regulation of the endoplasmic reticulum, as was previously

[1]Montreal Neurological Institute and Hospital, McGill University, Montréal, QC H3A 2B4, Canada; [2]Department of Human Genetics, McGill University, Montréal, QC H3A 0G4, Canada; [3]Department of Neurology and Neurosurgery, McGill University, Montréal, QC H3A 0G4, Canada; [4]Equipe de Recherche sur les Maladies Neurodégénératives, Medical School and Pharmacy, Mohammed V University, Rabat, BP 6527, Morocco; [5]Service de Neurophysiologie Clinique, Hôpital des Spécialités, Centre Hospitalier Ibn Sina, Université Mohammed V Souissi, Rabat, BP 6527, Morocco; [6]Centre de Recherche, Centre Hospitalier de l'Université de Montréal, Montréal, QC H2X 0A9, Canada; [7]Département de Pathologie et Biologie Cellulaire, Université de Montréal, Montréal, QC H3C 3J7, Canada; [8]Department of Pediatrics, Neuroscience and Mental Health Institute, University of Alberta, Edmonton, AB T6G 2R3, Canada; [9]Département de Neurosciences, Université de Montréal, Montréal, QC H3C 3J7, Canada; [10]Schulich School of Medicine and Dentistry, Western University, London, ON N6A 5C1, Canada; [11]Division of Neurology, Department of Pediatrics, University of Toronto, The Hospital for Sick Children, Toronto, ON M5G 1X8, Canada; [12]Division of Clinical and Metabolic Genetics, Department of Pediatrics, University of Toronto, The Hospital for Sick Children, Toronto, ON M5G 1X8, Canada; [13]Division of Neurology, Centre Hospitalier Universitaire de Québec, and Faculty of Medicine, Laval University, Quebec City, QC G1V 0A6, Canada; [14]Division of Neurology, University of Alberta, Edmonton, AB T6G 2R3, Canada
[15]These authors contributed equally to the work
*Correspondence: guy.rouleau@mcgill.ca
http://dx.doi.org/10.1016/j.ajhg.2016.04.002.

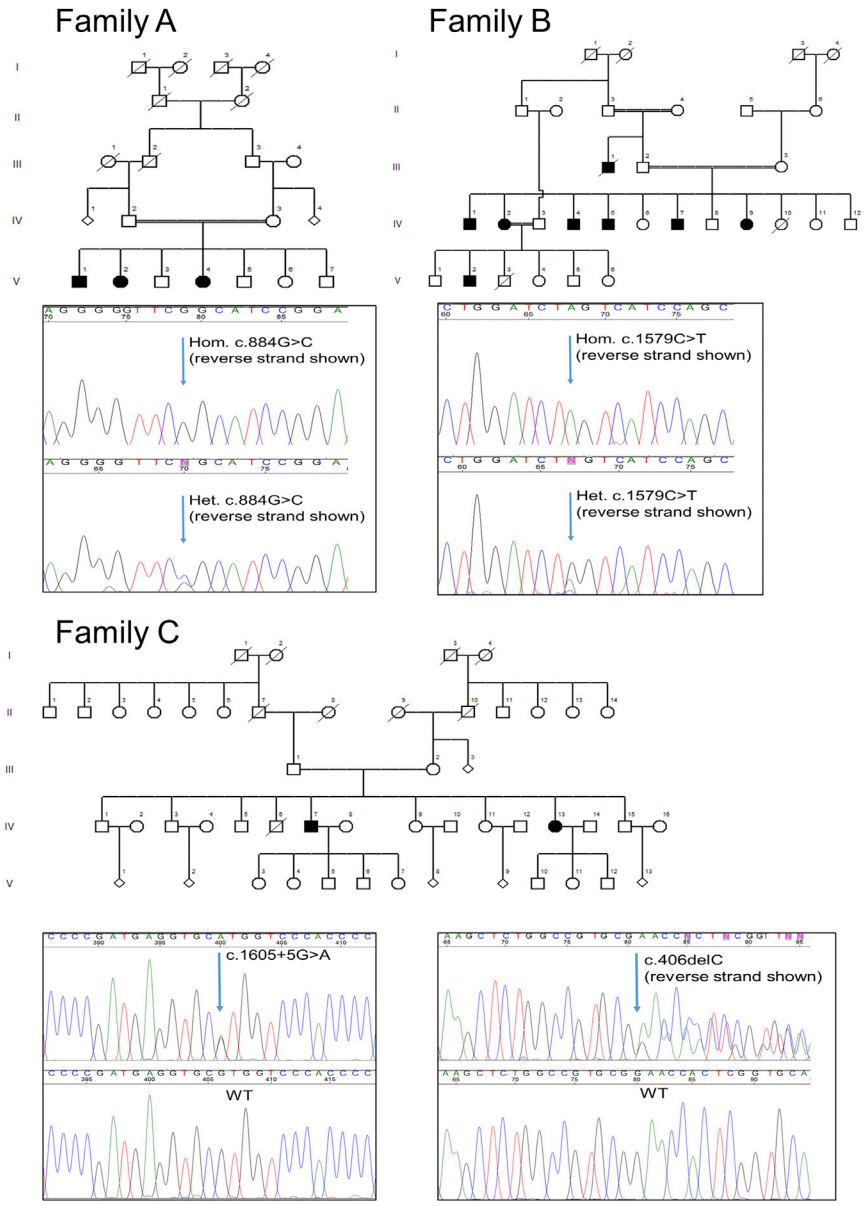


**Figure 1. Pedigrees and Mutations Detected in Three Families Affected by *CAPN1*-Associated HSP**

The three affected individuals from family A were homozygous for the c.884G>C (p.Arg295Pro) mutation, and all unaffected individuals with available DNA (IV-2, IV-3, V3, and V6) were heterozygous carriers of the mutation. In family B, all four affected individuals with available DNA (IV-1, IV-2, IV-5, and IV-9) were homozygous for the c.1579C>T stop variant (p.Gln527*), and all unaffected individuals with available DNA (III-2, III-3, and IV-11) were heterozygous carriers of the mutation. In family C, the two affected individuals were compound heterozygous for the frameshift c.406delC (p.Pro136Argfs*40) mutation and the splicing c.1605+5G>A mutation. Four more unaffected individuals were sequenced: III-1 (father of the affected individuals), III-2 (mother), IV-9 (sister), and IV-15 (brother). III-1 was heterozygous for the c.1605+5G>A mutation and a non-carrier of the frameshift mutation, and III-2 was heterozygous for the c.406delC mutation and a non-carrier of the splicing mutation. IV-9 was a non-carrier of both mutations, and IV-15 was a carrier of the c.1605+5G>A mutation and a non-carrier of the frameshift mutation.

reviewed.[3,6] In the current study, we used whole-exome sequencing (WES) to analyze three families affected by AR-HSP and identified homozygous or compound-heterozygous mutations in *CAPN1* (MIM: 114220) as the cause of HSP in these families. We further studied the effects of loss of function of *CAPN1* orthologs in *Caenorhabditis elegans*, *Drosophila melanogaster*, and *Danio rerio* models.

The three families (Figure 1) included two consanguineous Moroccan families (families A and B) and one family from Idaho and Utah (family C). Of note, the pedigree of family B is pseudo-dominant as a result of multiple intra-familial marriages. They live in a small village in northwestern Morocco, where many of the residents are related because of common ancestors. The clinical data on the affected individuals from these three families are detailed in Table 1. Families A and B were diagnosed and followed up by a neurologist in the Department of Clinical Neurophysiology at Centre Hospitalier Ibn Sina (Morocco), and members from family C were diagnosed and followed up by neurologists from Idaho and Utah. All individuals signed an informed-consent form before entering the study, and the study design and protocols were approved by the institutional review boards. Table 1 details the clinical characteristics of eight individuals with available clinical data, and detailed case reports are provided in the Supplemental Note. The average age at onset was 28.5 years (±8.05, range = 19–39), and the affected individuals presented with symptoms of complicated HSP. In addition to showing lower-extremity spasticity and hyperreflexia, seven of the eight individuals had upper-extremity hyperreflexia, six had dysarthria, and three had ataxia. Six individuals had foot deformities—five with the typical pes cavus and one with pes valgus. Abnormal bladder function was reported in two individuals. No seizures were reported. Overall, the motor impairment was mild to moderate, and two of the individuals (IV-2 in family B and IV-13 in family C) had started using a cane to aid walking. No vision abnormalities were reported or identified in the neurological examinations. Blood samples for DNA analysis were available from nine affected individuals (V-1, V-2, and V-4 in family A, IV-1, IV-2, IV-5, and IV-9 in family B, and IV-7 and IV-13 in family C; Figure 1), and all nine samples went through

**Table 1. Clinical Features of the Affected Individuals with Autosomal-Recessive HSP and Available Clinical Data**

| | Family A | Family B | | | | | Family C | |
|---|---|---|---|---|---|---|---|---|
| | V-2 | IV-1 | IV-2 | IV-4 | IV-5 | IV-9 | IV-7 | IV-13 |
| Age at onset (years) | 20 | 35 | 36 | 22 | 39 | 24 | 33 | 19 |
| Age at examination (years) | 31 | 47 | 44 | 42 | 40 | 30 | 35 | 22 |
| Lower-extremity spasticity | + | + | + | + | + | + | + | + |
| Lower-extremity weakness | + | + | + | + | − | − | ? | + |
| Lower-extremity hyperreflexia | + | + | + | + | + | + | ? | + |
| Extensor plantar response | + | + | + | + | − | + | − | + |
| Abnormal bladder function | + | − | − | − | − | − | − | + |
| Foot deformity | +[a] | − | +[b] | +[b] | − | +[b] | +[b] | +[b] |
| Ataxia | − | − | + | − | + | − | − | + |
| Other symptoms and signs | dysarthria, upper-extremity hyperreflexia | dysarthria, upper-extremity hyperreflexia, sensory abnormalities, peripheral neuropathy | dysarthria, upper-extremity hyperreflexia, peripheral neuropathy, gait ataxia, upper-extremity ataxia, scoliosis | dysarthria, upper-extremity hyperreflexia, amyotrophy | ocular movement abnormalities, dysarthria, upper-extremity hyperreflexia and gait ataxia, amyotrophy | dysarthria, upper-extremity hyperreflexia | ankle clonus | mild gait ataxia, upper-extremity hyperreflexia, bilateral ankle clonus |

[a]Pes valgus.
[b]Pes cavus.

WES. Additional samples from unaffected individuals were available from four individuals in family A (IV-2, IV-3, V-3, and V-6), three individuals in family B (III-2, III-3, and IV-11), and four individuals in family C (III-1, III-2, IV-9, and IV-15). These additional samples were used for validation and segregation analysis of the mutations. DNA was extracted according to a standard salting-out protocol and was captured for WES with the Agilent SureSelect Human All Exon V4 Kit according to the manufacturer's (Agilent Technologies) instructions. The captured DNA was sequenced with an Illumina HiSeq 2000 (2 × 100 bp, three samples per lane) at the Innovation Genome Center of McGill University and Genome Québec. Sequence processing, alignment, and variant calling were performed with the Burrows-Wheeler Aligner,[9] the Genome Analysis Toolkit (v.4),[10] and ANNOVAR.[11] After annotation, data on the detected variants were extracted from publicly available databases: the 1000 Genomes Project,[12] the National Heart, Lung, and Blood Institute Exome Sequencing Project (ESP) Exome Variant Server (EVS), the Exome Aggregation Consortium (ExAC) Browser, and dbSNP132. In addition, the frequencies of these variants were calculated in our in-house dataset of over 1,600 samples that had undergone WES. To estimate the potential effects of the mutation, we used the online prediction and conservation tools SIFT,[13] PolyPhen-2,[14] MutationTaster,[15] PhyloP,[16] and GERP++.[17] Details on the filtering process can be found in the Table S2. In order to validate and examine segregation of the candidate mutations with the disease, we used specific primers to amplify DNA from all affected and unaffected family members with available samples and sequenced them by Sanger sequencing (Applied Biosystem's 3730xl DNA Analyzer technology; primers are detailed in Table S1).

The average coverage of the nine samples that were sequenced by WES was 129×, 99% of the bases had a coverage > 10×, and 97% had a coverage > 20×. In order to identify potential causative mutations, we excluded all variants with an allele frequency > 0.005 in the 1000 Genomes Project, EVS, or dbSNP132 and variants that were already found in our in-house dataset. In an effort to include only nonsynonymous, frameshift, stop, and splice-site mutations, we subsequently removed synonymous, 5′ UTR, 3′ UTR, and intronic variants that were not within the six nucleotides at splice sites. Further filtering was done on the basis of predicted deleterious effects and conservation. In families A and B, homozygous mutations were considered, and in family C, both homozygous and compound-heterozygous variants were considered (Table S2). No mutations in exons covered by the exome sequencing in known or suspected HSP-associated genes segregated with the disease in any of the families. In the three families, mutations in only one gene, *CAPN1*,

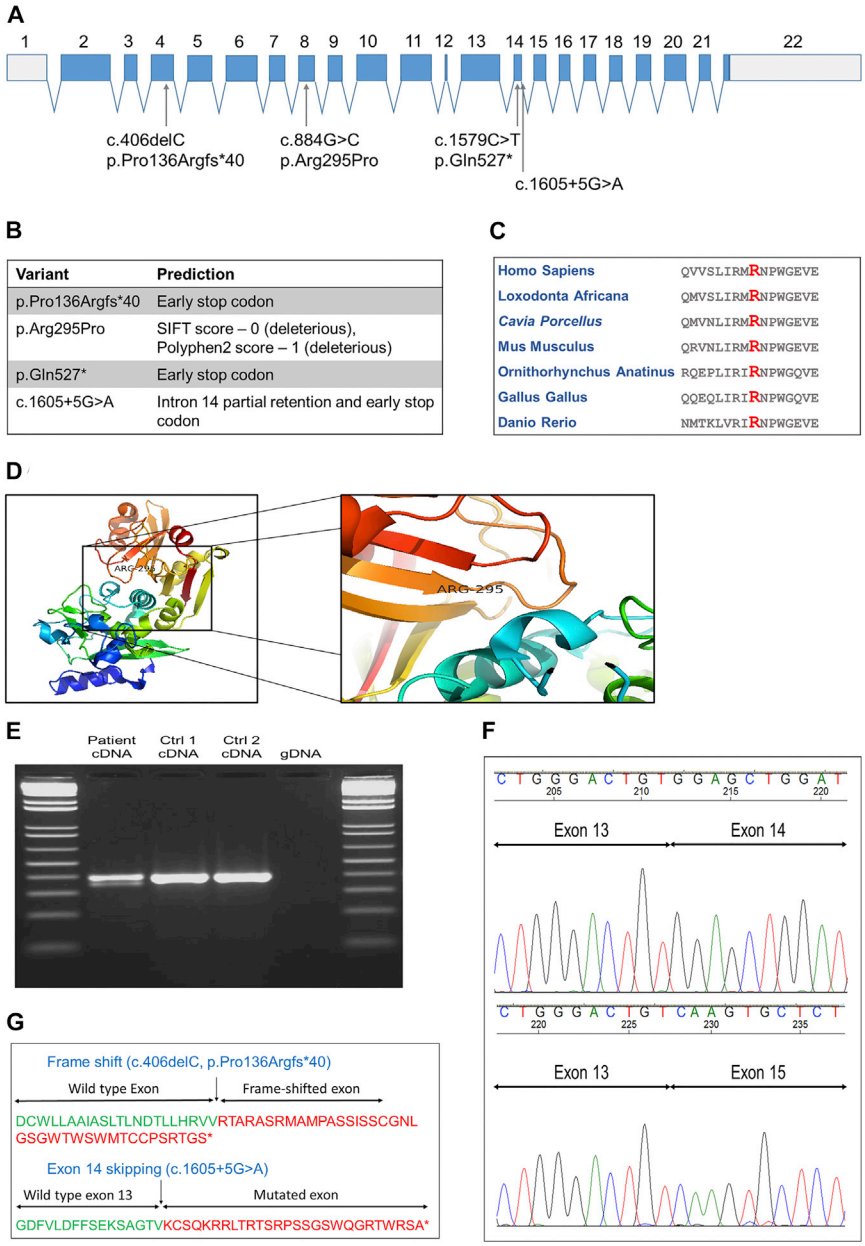


**Figure 2. Characteristics and Predictions of the *CAPN1* Mutations**

(A) Structure of *CAPN1* and the locations of the four mutations identified in the current study.

(B) Functional predictions of all four mutations.

(C) Conservation of Arg295 in different species. With a GERP++ score > 2, this amino acid is highly conserved.

(D) Three-dimensional model of calpain 1 and the location of the p.Arg295Pro substitution at the end of a β strand and just before the active site at p.Asn296 (PDB: 1ZCM).

(E) cDNA produced from lymphoblasts of an affected individual and two control individuals, around exon 14. In the left lane, two cDNA products were observed, suggesting that the c.1605+5G>A mutation affected splicing.

(F) Sequencing of cDNA from RT-PCR of the RNA around splicing mutation c.1605+5G>A demonstrated that this mutation caused the skipping of exon 14.

(G) Effects of the frameshift mutation c.406delC (p.Pro136Argfs*40) (top) and the splicing mutation c.1605+5G>A (bottom) on calpain 1.

segregated with the disease (spastic paraplegia 76 [SPG76 (MIM: 616907)]) after filtering (Figure 1). In family A, the three affected individuals were homozygous for a missense mutation in exon 8 of *CAPN1*: c.884G>C (GenBank: NM_005186), leading to a p.Arg295Pro substitution, which is predicted to be deleterious (SIFT score 0, PolyPhen-2 score 1) and highly conserved (GERP++ score > 2; Figure 2C). This substitution is located next to an active site in position 296, the amino acid asparagine, which is a critical $Ca^{2+}$ binding site[18,19] at the end of a β strand (Figure 2D). In family B, the four affected individuals were homozygous for a nonsense mutation in exon 14: c.1579C>T (GenBank: NM_005186), resulting in a p.Gln527* early termination of the protein. Homozygosity mapping of the seven individuals from these two families confirmed that a region on chromosome 11, spanning 3.5 Mb and containing *CAPN1*, is the only shared homozygous region. In family C, the two affected individuals were compound heterozygous for a frameshift mutation on exon 4 (c.406delC [p.Pro136Argfs*40]; Figure 2G) and a splicing mutation (c.1605+5G>A; Figures 2E–2G). None of these variants from the three families were identified in the 1000 Genome Project, ESP, or our in-house dataset of >1,600 exome-sequencing samples. The coding variants were also not detected in the ExAC Browser, and the c.1605+5G>A splice-site mutation had a frequency of 0.0001. All mutations were validated via Sanger sequencing, and all the available DNA samples from family members were also sequenced. In family A, the two parents (IV-2 and IV-3; Figure 1) and two siblings (V-3 and V-6) of the affected individuals were all heterozygous for the *CAPN1* c.884G>C (p.Arg295Pro) mutation. In family B, the two parents (III-2 and III-3) and one sibling (IV-11) of the four individuals sequenced by WES were all heterozygous carriers of the *CAPN1* c.1579C>T (p.Gln527*) mutation. In family C, both parents (III-1 and III-2) and two siblings (IV-9 and IV-15) were sequenced. The father, III-1, was a heterozygous carrier of the c.1605+5G>A mutation, and the mother, III-2, was a heterozygous carrier of the c.406delC mutation, confirming phasing. Sibling IV-9 was a non-carrier of both variants, and IV-15 was a heterozygous carrier of the c.1605+5G>A

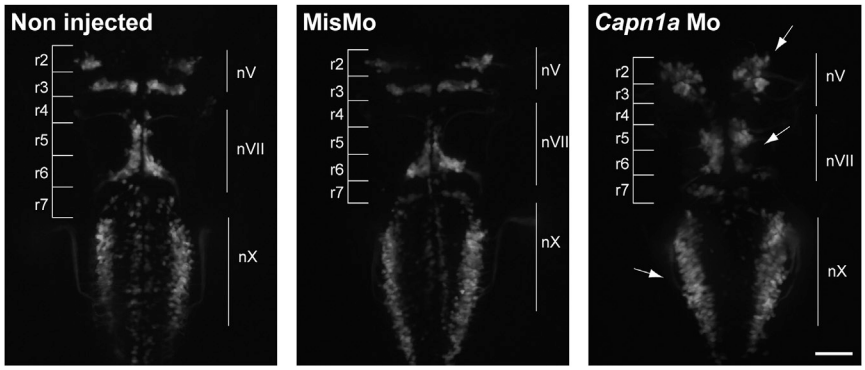


**Figure 3. Branchiomotor Neurons of *capn1a*-Mo-Injected Embryos Display Abnormal Migration**
Abnormal development and migration of both nV (trigeminal) and nVII (facial) branchiomotor neurons in 2 dpf Islet1:GFP embryos either not injected or injected with the mismatch Mo (MisMo) or *capn1a* Mo. Arrows indicate abnormally located cell bodies. R stands for "rhombomere." The scale bar represents 50 μm.

mutation. To examine the predicted effect of the splice-site c.1605+5G>A mutation, we produced RNA from immortalized lymphoblasts from individual IV-7 (family C) and from healthy family members, and we produced cDNA with the Invitrogen SuperScript III Reverse Transcriptase Kit (Invitrogen). Specific primers (forward 5′-ACTATTGG CTTCGCGGTCTA-3′ and reverse 5′-ATTGTCCGCAACTCC TTCAC-3′) were designed to amplify the cDNA around the c.1605+5G>A mutation with a cDNA amplicon length of 389 bp (DNA amplicon length = 3,405 bp). Individual IV-7 had two copies of cDNA with different lengths around the c.1605+5G>A splice-site mutation (Figure 2E). Sequencing of the cDNA after separation on gel demonstrated that this splice variant results in exon 14 skipping and an early stop codon (Figures 2E–2G).

RNAi knockdown of *clp-1*, the *C. elegans* ortholog of *CAPN1*, led to neurodegeneration of GABAergic motor neurons and an age-dependent paralysis phenotype (see Figure S1 for details on the experiments and results). Similarly, loss of function of the *CAPN1* ortholog in *D. melanogaster* led to locomotor defects and axonal abnormalities (see Figures S2 and S3 for details on the experiments and results). RNAi against the *D. melanogaster* ortholog, *calpain B*, led to age-dependent negative geotaxis (Figure S2). Defects in axons were observed in transgenic flies expressing *calpain B* with the pan-neuronal driver Elav. Axons appeared to have larger diameters and increased levels of acetylated tubulin (Figure S3).

Zebrafish (*D. rerio*) embryos were collected and staged according to standard methods.[20] The local animal care committee at the Centre de Recherche du Centre Hospitalier de l'Université de Montréal, having received the protocol relevant to this project and relating to animal care and treatment, certified that the care and treatment of animals was in accordance with the guidelines and principles of the Canadian Council on Animal Care. Zebrafish embryos (no adults were used) are insentient to pain. Similarly to the findings in *D. melanogaster*, Figure S4 demonstrates clusters of acetylated tubulin in zebrafish with mutant *calpain 1a* (*capn1a*). Increased acetylated tubulin is associated with hyperstabilization of microtubules and has previously been associated with *SPAST* mutations. Zebrafish *capn1a* and *calpain 1b* (*capn1b*) both encode proteins that are orthologs of the human CAPN1.[21] We used a morpholino oligonucleotide (Mo) against each gene to model the loss of function of *CAPN1*. The *capn1a* Mo, but not the *capn1b* Mo, led to a phenotype (data not shown). Details on the knockdown of the zebrafish calpains, morphology measurements, and imaging are in Figure S5 legend. The *capn1a* Mo resulted in several developmental defects visible at 2 days postfertilization (dpf), and a moderate to severe phenotype was exhibited by 78% of injected embryos at 5 dpf, indicating that these defects are long lasting (Figure S5). Knockdown with the *capn1a* Mo was confirmed in western blots at 48 hr postfertilization (hpf) (Figure S6). However, co-injecting the human wild-type *CAPN1* mRNA (up to 500 pg of RNA) in wild-type and Mo-injected eggs failed to show a toxic effect of the RNA on its own or a rescue of the Mo-induced phenotype. By western blotting (Figure S6), the zebrafish and human calpain 1 proteins showed exclusive patterns that explain the failed rescue. Specifically, the human protein was detected at 24 hpf, but not at 48 hpf, whereas the zebrafish protein was detected only later at 48 hpf. Thus, the early expression of human mRNA could very well have failed to rescue the later knockdown phenotype. Because of the lack of rescue, the role of the CAPN1 p.Arg295Pro substitution could not be established in this model, and other models will be necessary for examining the effect of this substitution. Because *capn1a* is mainly expressed in the brain starting at 24 hpf,[21] we injected *capn1a* Mo in the Islet1::GFP transgenic fish expressing GFP in the motor neurons, including the branchiomotor neurons. We observed a disorganization of these motor neurons in comparison to those of the control, as well as migration defects of the nV trigeminal nuclei in rhombomeres 2 and 3 (r2 and r3, respectively) and of the VII facial branchiomotor neuronal cell bodies, which had not fully migrated from r4 to r6. Furthermore, the vagal motor neurons had an aberrant positioning and spacing, probably because of a defect in cell motility (Figure 3).

Growing axons in the brain and spinal cord were then observed with an antibody against acetylated tubulin. The microtubule network in the brain of *capn1a*-Mo-injected embryos (Figures 4B and 4D) appeared to be following a different pattern than in the morphants injected with

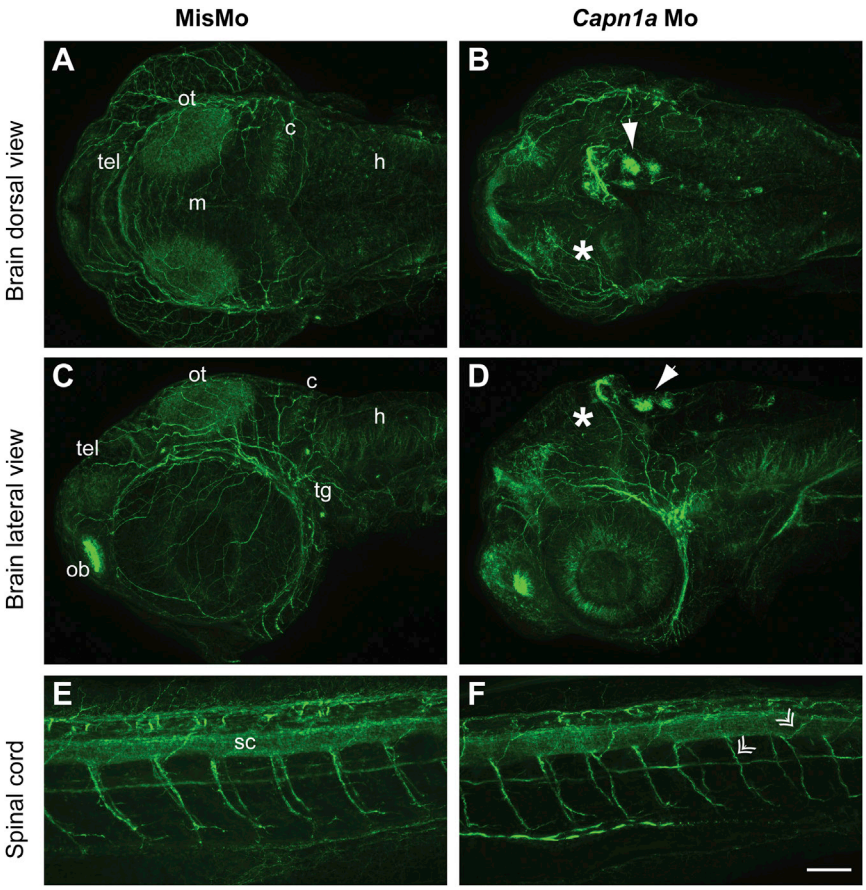


**Figure 4. Disorganization of the Microtubule Network in the Brain of *capn1a* Morphants**

(A and B) Dorsal view of Z-projections of acetylated-tubulin staining in the brain of embryos injected with MisMo (A) and *capn1a* Mo (B).

(C and D) Lateral view of Z-projections of acetylated-tubulin staining in the brain of embryos injected with MisMo (C) and *capn1a* Mo (D). The dorsal side is toward the top of the image.

(E and F) Spinal cord, along the six to eight somites spanning the anus of the embryos, of embryos injected with MisMo (E) and *capn1a* Mo (F). The dorsal side is toward the top of the image. Double arrows point toward thinner and disorganized motor neuron axons of the *capn1a* morphants. Solid white arrows show the clusters of tubulin. Asterisks show the fainter staining of the optic tectum of *capn1a* morphants. In all images, caudal is to the left. The scale bar represents 60 μm. Abbreviations are as follows: ot, optic tectum; tg, trigeminal ganglion; h, hindbrain; c, cerebellum; m, midbrain; tel, telencephalon; ob, olfactory bulb; and sc, spinal cord.

mismatch Mo (MisMo) (Figures 4A and 4C). Reduced acetylated-tubulin staining could be observed at the level of the optic tectum and cerebellum, whereas a stronger staining was found in the telencephalon. Strikingly, clusters of acetylated tubulin could be observed in some cells in the dorsalmost part of the brain (Figures 4B and 4D). Furthermore, acetylated-tubulin staining in the spinal cord demonstrated that microtubules in the motor neuron axons were thinner and more disorganized, although this effect was not as strong as in the brain (Figures 4E and 4F). Although the exact pattern varied from embryo to embryo, the vast majority of embryos injected with the *capn1a* Mo (29/30) exhibited similar staining, whereas the controls did not (both non-injected embryos [0/30, data not shown] and MisMo-injected embryos [0/30]).

The current study demonstrates that rare homozygous or compound-heterozygous mutations in *CAPN1* cause a complicated form of HSP. Most of the affected individuals from the three families suffer from additional neurological symptoms in addition to the typical spasticity of the lower limbs, such as upper-extremity hyperreflexia, dysarthria, and gait ataxia (Table 1). These features are also seen in other autosomal-recessive forms of HSP. For example, individuals with AR-HSP caused by mutations in *SPG7* (MIM: 607259) often present with phenotypes very similar to those described in the current study, including symptoms such as dysarthria, ataxia, upper-extremity hyperreflexia, amyotrophy, pes cavus, and sensory neuropathy.[22–24] Similar phenotypes have also been observed in individuals with mutations in *KIF1A* (MIM: 610357)[25,26] and other forms of AR-HSP.[27] In our dataset that includes 405 HSP-affected individuals from 252 families, *CAPN1* mutations account for 2.2% of the affected individuals and 1.2% of the families. However, this is an overestimation, given that our dataset does not include families in whom the genetic cause was established prior to our study. Therefore, these values should be considered as maximal. *CAPN1*, located in chromosomal region 11q13, encodes calpain 1, also known as the large subunit of μ-calpain, a calcium-activated cysteine protease that is widely present in the CNS.[28] Calpain 1 is probably important for several functions in the CNS, but its exact role in humans is still not clear. Calpain 1 is involved in synaptic plasticity,[29–32] and several mechanisms for its function have been suggested in animal models. For example, it was shown that calpain interacts with CDK5 and NR2B to control NMDA-receptor degradation and synaptic plasticity.[33] Another study suggested that calpain 1 can affect synaptic plasticity through degradation of its substrate, glutamate receptor-interacting protein, thus affecting AMPA receptors.[34] However, there are contradicting results regarding the roles of calpains in neuroprotection and neurodegeneration, given that several studies suggest that calpain inhibition might be neuroprotective.[35,36] A recent study might offer a solution for this contradiction by demonstrating that selective knockout of *Capn1* (encoding μ-calpain) leads to increased neurotoxicity and that its activity is in fact neuroprotective, whereas

knockout of *Capn2* (encoding m-calpain) is neuroprotective.[37] Our animal models support the neuroprotective role of *calpain 1*, given that its knockdown led to neurodegeneration or disorganization of neurons. Therefore, it is likely that different forms of calpain have different or even opposing effects on neurodegeneration and that calpains might have different effects in different disorders and different species.

This can be further exemplified by calpain-1-deficient mice, which have normal gross brain development and architecture yet have reduced spine density and ramifications of basal and apical dendrites in hippocampal CA1 pyramidal neurons, emphasizing the importance of calpain 1 in regulation and organization of dendritic trees in hippocampal CA1 neurons.[38] Moreover, a knockout mouse model of another HSP-related gene, *CYP7B1* (MIM: 270800), also resulted in the lack of an obvious CNS phenotype.[39] These observations are comparable to human HSP, because in humans too, brain imaging and development often seem to be normal, whereas affected individuals in fact suffer from axonal degeneration of the descending corticospinal tract and ascending sensory fibers.[5] Interestingly, loss-of-function mutations in *CAPN1* have been suggested to cause spinocerebellar ataxia in dogs,[40] a neurological disorder that shares features with HSP. Of note, all but one of the individuals in our studies have cerebellar signs such as dysarthria and ataxia.

In zebrafish embryos, knockdown of *calpain 1a* resulted in disruption of brain development, particularly of branchiomotor neuron migration and positioning. The microtubule network in the brain was disorganized, such that some regions showed an abnormal accumulation of axonal acetylated tubulin, whereas others were depleted. This disruption of the microtubule network was more prominent in the brain, but motor neuron axons in the spinal cord were also moderately affected. The presence of large clusters of acetylated tubulin in some cells of the brain is specific to the knockdown of *calpain 1a*, given that it was not observed in other embryos exhibiting hydrocephalus and migration defects in branchiomotor neurons.[41,42] Similarly, the neuromuscular junction of *D. melanogaster* with *calpain B* knockdown showed abnormal levels of acetylated tubulin. Interestingly, similar observations were reported for spastin, encoded by *SPAST*, in which mutations are the most common genetic cause of HSP.[43,44] This suggests that the two genes might be involved in a similar mechanism; however, whether *CAPN1*- and *SPG4*-associated HSP share the same mechanisms is still to be determined.

Fully understanding the roles of the different calpains in general, and calpain 1 specifically, will require more studies, especially in human tissues. Such studies should focus on isolating the effects of specific calpains on neurodegeneration and neuroprotection. In addition, efforts should be made to identify more individuals with *CAPN1*-associated HSP to expand our knowledge of its phenotype.

## Supplemental Data

Supplemental Data include a Supplemental Note, six figures, and three tables and can be found with this article online at http://dx.doi.org/10.1016/j.ajhg.2016.04.002.

## Acknowledgments

We thank the families for their participation. This study was funded by an Emerging Team Grant (RN127580-260005) from the Canadian Institutes for Health Research (CIHR) in collaboration with the Canadian Organization for Rare Disorders. This work was done as a part of a Canadian collaboration to study hereditary spastic paraplegia (CanHSP). Z.G.-O. is supported by a postdoctoral fellowship from the CIHR. P.D. holds a Canada Research Chair in Neuroscience, and A.L. is the recipient of a CIHR ALS Canada Doctoral Research Award. G.A.R. holds a Canada Research Chair in Genetics of the Nervous System and the Wilder Penfield Chair in Neurosciences. We thank Dr. Hitoshi Okamoto for the zebrafish Islet-1 transgenic line. We thank Helene Catoire, Pascale Hince, Cynthia Bourassa, Amirthagowri Ambalavanan, and Cathy Mirarchi for their assistance.

Received: October 18, 2015
Accepted: April 5, 2016
Published: May 5, 2016

## Web Resources

dbSNP132, http://www.ncbi.nlm.nih.gov/projects/SNP/snp_summary.cgi?build_id=132
ExAC Browser, http://exac.broadinstitute.org/
GERP++, http://mendel.stanford.edu/SidowLab/downloads/gerp/
MutationTaster, http://www.mutationtaster.org/
NHLBI Exome Sequencing Project (ESP) Exome Variant Server, http://evs.gs.washington.edu/EVS/
OMIM, http://www.omim.org/
PhyloP, http://compgen.cshl.edu/phast/
PolyPhen-2, http://genetics.bwh.harvard.edu/pph2/
RefSeq, http://www.ncbi.nlm.nih.gov/refseq/
SIFT, http://sift.jcvi.org/

## References

1. McDermott, C., White, K., Bushby, K., and Shaw, P. (2000). Hereditary spastic paraparesis: a review of new developments. J. Neurol. Neurosurg. Psychiatry *69*, 150–160.
2. Salinas, S., Proukakis, C., Crosby, A., and Warner, T.T. (2008). Hereditary spastic paraplegia: clinical features and pathogenetic mechanisms. Lancet Neurol. *7*, 1127–1138.
3. Blackstone, C. (2012). Cellular pathways of hereditary spastic paraplegia. Annu. Rev. Neurosci. *35*, 25–47.
4. Lo Giudice, T., Lombardi, F., Santorelli, F.M., Kawarai, T., and Orlacchio, A. (2014). Hereditary spastic paraplegia: clinical-genetic characteristics and evolving molecular mechanisms. Exp. Neurol. *261*, 518–539.
5. Deluca, G.C., Ebers, G.C., and Esiri, M.M. (2004). The extent of axonal loss in the long tracts in hereditary spastic paraplegia. Neuropathol. Appl. Neurobiol. *30*, 576–584.
6. Noreau, A., Dion, P.A., and Rouleau, G.A. (2014). Molecular aspects of hereditary spastic paraplegia. Exp. Cell Res. *325*, 18–26.

7. Novarino, G., Fenstermaker, A.G., Zaki, M.S., Hofree, M., Silhavy, J.L., Heiberg, A.D., Abdellateef, M., Rosti, B., Scott, E., Mansour, L., et al. (2014). Exome sequencing links corticospinal motor neuron disease to common neurodegenerative disorders. Science *343*, 506–511.
8. Hazan, J., Fonknechten, N., Mavel, D., Paternotte, C., Samson, D., Artiguenave, F., Davoine, C.S., Cruaud, C., Dürr, A., Wincker, P., et al. (1999). Spastin, a new AAA protein, is altered in the most frequent form of autosomal dominant spastic paraplegia. Nat. Genet. *23*, 296–303.
9. Li, H., and Durbin, R. (2009). Fast and accurate short read alignment with Burrows-Wheeler transform. Bioinformatics *25*, 1754–1760.
10. McKenna, A., Hanna, M., Banks, E., Sivachenko, A., Cibulskis, K., Kernytsky, A., Garimella, K., Altshuler, D., Gabriel, S., Daly, M., and DePristo, M.A. (2010). The Genome Analysis Toolkit: a MapReduce framework for analyzing next-generation DNA sequencing data. Genome Res. *20*, 1297–1303.
11. Wang, K., Li, M., and Hakonarson, H. (2010). ANNOVAR: functional annotation of genetic variants from high-throughput sequencing data. Nucleic Acids Res. *38*, e164.
12. Abecasis, G.R., Auton, A., Brooks, L.D., DePristo, M.A., Durbin, R.M., Handsaker, R.E., Kang, H.M., Marth, G.T., and McVean, G.A.; 1000 Genomes Project Consortium (2012). An integrated map of genetic variation from 1,092 human genomes. Nature *491*, 56–65.
13. Kumar, P., Henikoff, S., and Ng, P.C. (2009). Predicting the effects of coding non-synonymous variants on protein function using the SIFT algorithm. Nat. Protoc. *4*, 1073–1081.
14. Adzhubei, I.A., Schmidt, S., Peshkin, L., Ramensky, V.E., Gerasimova, A., Bork, P., Kondrashov, A.S., and Sunyaev, S.R. (2010). A method and server for predicting damaging missense mutations. Nat. Methods *7*, 248–249.
15. Schwarz, J.M., Cooper, D.N., Schuelke, M., and Seelow, D. (2014). MutationTaster2: mutation prediction for the deep-sequencing age. Nat. Methods *11*, 361–362.
16. Pollard, K.S., Hubisz, M.J., Rosenbloom, K.R., and Siepel, A. (2010). Detection of nonneutral substitution rates on mammalian phylogenies. Genome Res. *20*, 110–121.
17. Davydov, E.V., Goode, D.L., Sirota, M., Cooper, G.M., Sidow, A., and Batzoglou, S. (2010). Identifying a high fraction of the human genome to be under selective constraint using GERP++. PLoS Comput. Biol. *6*, e1001025.
18. Khorchid, A., and Ikura, M. (2002). How calpain is activated by calcium. Nat. Struct. Biol. *9*, 239–241.
19. Moldoveanu, T., Hosfield, C.M., Lim, D., Elce, J.S., Jia, Z., and Davies, P.L. (2002). A Ca(2+) switch aligns the active site of calpain. Cell *108*, 649–660.
20. Kimmel, C.B., Ballard, W.W., Kimmel, S.R., Ullmann, B., and Schilling, T.F. (1995). Stages of embryonic development of the zebrafish. Dev. Dyn. *203*, 253–310.
21. Lepage, S.E., and Bruce, A.E. (2008). Characterization and comparative expression of zebrafish calpain system genes during early development. Dev. Dyn. *237*, 819–829.
22. Casari, G., and Marconi, R. (1993). Spastic Paraplegia 7. In GeneReviews, R.A. Pagon, M.P. Adam, H.H. Ardinger, S.E. Wallace, A. Amemiya, L.J.H. Bean, T.D. Bird, C.R. Dolan, C.T. Fong, R.J.H. Smith, et al., eds.
23. Wilkinson, P.A., Crosby, A.H., Turner, C., Bradley, L.J., Ginsberg, L., Wood, N.W., Schapira, A.H., and Warner, T.T. (2004). A clinical, genetic and biochemical study of SPG7 mutations in hereditary spastic paraplegia. Brain *127*, 973–980.
24. Brugman, F., Scheffer, H., Wokke, J.H., Nillesen, W.M., de Visser, M., Aronica, E., Veldink, J.H., and van den Berg, L.H. (2008). Paraplegin mutations in sporadic adult-onset upper motor neuron syndromes. Neurology *71*, 1500–1505.
25. Klebe, S., Azzedine, H., Durr, A., Bastien, P., Bouslam, N., Elleuch, N., Forlani, S., Charon, C., Koenig, M., Melki, J., et al. (2006). Autosomal recessive spastic paraplegia (SPG30) with mild ataxia and sensory neuropathy maps to chromosome 2q37.3. Brain *129*, 1456–1462.
26. Klebe, S., Lossos, A., Azzedine, H., Mundwiller, E., Sheffer, R., Gaussen, M., Marelli, C., Nawara, M., Carpentier, W., Meyer, V., et al. (2012). KIF1A missense mutations in SPG30, an autosomal recessive spastic paraplegia: distinct phenotypes according to the nature of the mutations. Eur. J. Hum. Genet. *20*, 645–649.
27. Coutinho, P., Barros, J., Zemmouri, R., Guimarães, J., Alves, C., Chorão, R., Lourenço, E., Ribeiro, P., Loureiro, J.L., Santos, J.V., et al. (1999). Clinical heterogeneity of autosomal recessive spastic paraplegias: analysis of 106 patients in 46 families. Arch. Neurol. *56*, 943–949.
28. Goll, D.E., Thompson, V.F., Li, H., Wei, W., and Cong, J. (2003). The calpain system. Physiol. Rev. *83*, 731–801.
29. Lynch, G., and Baudry, M. (1984). The biochemistry of memory: a new and specific hypothesis. Science *224*, 1057–1063.
30. Denny, J.B., Polan-Curtain, J., Ghuman, A., Wayner, M.J., and Armstrong, D.L. (1990). Calpain inhibitors block long-term potentiation. Brain Res. *534*, 317–320.
31. Vanderklish, P., Bednarski, E., and Lynch, G. (1996). Translational suppression of calpain blocks long-term potentiation. Learn. Mem. *3*, 209–217.
32. Zadran, S., Jourdi, H., Rostamiani, K., Qin, Q., Bi, X., and Baudry, M. (2010). Brain-derived neurotrophic factor and epidermal growth factor activate neuronal m-calpain via mitogen-activated protein kinase-dependent phosphorylation. J. Neurosci. *30*, 1086–1095.
33. Hawasli, A.H., Benavides, D.R., Nguyen, C., Kansy, J.W., Hayashi, K., Chambon, P., Greengard, P., Powell, C.M., Cooper, D.C., and Bibb, J.A. (2007). Cyclin-dependent kinase 5 governs learning and synaptic plasticity via control of NMDAR degradation. Nat. Neurosci. *10*, 880–886.
34. Lu, X., Wyszynski, M., Sheng, M., and Baudry, M. (2001). Proteolysis of glutamate receptor-interacting protein by calpain in rat brain: implications for synaptic plasticity. J. Neurochem. *77*, 1553–1560.
35. O'Hanlon, G.M., Humphreys, P.D., Goldman, R.S., Halstead, S.K., Bullens, R.W., Plomp, J.J., Ushkaryov, Y., and Willison, H.J. (2003). Calpain inhibitors protect against axonal degeneration in a model of anti-ganglioside antibody-mediated motor nerve terminal injury. Brain *126*, 2497–2509.
36. Crocker, S.J., Smith, P.D., Jackson-Lewis, V., Lamba, W.R., Hayley, S.P., Grimm, E., Callaghan, S.M., Slack, R.S., Melloni, E., Przedborski, S., et al. (2003). Inhibition of calpains prevents neuronal and behavioral deficits in an MPTP mouse model of Parkinson's disease. J. Neurosci. *23*, 4081–4091.
37. Wang, Y., Briz, V., Chishti, A., Bi, X., and Baudry, M. (2013). Distinct roles for μ-calpain and m-calpain in synaptic NMDAR-mediated neuroprotection and extrasynaptic NMDAR-mediated neurodegeneration. J. Neurosci. *33*, 18880–18892.
38. Amini, M., Ma, C.L., Farazifard, R., Zhu, G., Zhang, Y., Vanderluit, J., Zoltewicz, J.S., Hage, F., Savitt, J.M., Lagace, D.C., et al. (2013). Conditional disruption of calpain in the CNS alters

dendrite morphology, impairs LTP, and promotes neuronal survival following injury. J. Neurosci. *33*, 5773–5784.
39. Li-Hawkins, J., Lund, E.G., Turley, S.D., and Russell, D.W. (2000). Disruption of the oxysterol 7alpha-hydroxylase gene in mice. J. Biol. Chem. *275*, 16536–16542.
40. Forman, O.P., De Risio, L., and Mellersh, C.S. (2013). Missense mutation in CAPN1 is associated with spinocerebellar ataxia in the Parson Russell Terrier dog breed. PLoS ONE *8*, e64627.
41. Chen, H.L., Yuh, C.H., and Wu, K.K. (2010). Nestin is essential for zebrafish brain and eye development through control of progenitor cell apoptosis. PLoS ONE *5*, e9318.
42. Hanington, P.C., Patten, S.A., Reaume, L.M., Waskiewicz, A.J., Belosevic, M., and Ali, D.W. (2008). Analysis of leukemia inhibitory factor and leukemia inhibitory factor receptor in embryonic and adult zebrafish (Danio rerio). Dev. Biol. *314*, 250–260.
43. Denton, K.R., Lei, L., Grenier, J., Rodionov, V., Blackstone, C., and Li, X.J. (2014). Loss of spastin function results in disease-specific axonal defects in human pluripotent stem cell-based models of hereditary spastic paraplegia. Stem Cells *32*, 414–423.
44. Trotta, N., Orso, G., Rossetto, M.G., Daga, A., and Broadie, K. (2004). The hereditary spastic paraplegia gene, spastin, regulates microtubule stability to modulate synaptic structure and function. Curr. Biol. *14*, 1135–1147.

**The American Journal of Human Genetics, Volume *98***

## Supplemental Data

# Mutations in *CAPN1* Cause Autosomal-Recessive Hereditary Spastic Paraplegia

**Ziv Gan-Or, Naima Bouslam, Nazha Birouk, Alexandra Lissouba, Daniel B. Chambers, Julie Vérièpe, Alaura Androschuck, Sandra B. Laurent, Daniel Rochefort, Dan Spiegelman, Alexandre Dionne-Laporte, Anna Szuto, Meijiang Liao, Denise A. Figlewicz, Ahmed Bouhouche, Ali Benomar, Mohamed Yahyaoui, Reda Ouazzani, Grace Yoon, Nicolas Dupré, Oksana Suchowersky, Francois V. Bolduc, J. Alex Parker, Patrick A. Dion, Pierre Drapeau, Guy A. Rouleau, and Bouchra Ouled Amar Bencheikh**

**Supplemental Note: Case Reports**

## Family A

### Individual V-2

Individual V-2 presented with onset of progressive walking difficulties at the age of 20. She was initially examined by us at the age of 31 years, at the time complaining of gait difficulty and urinary frequency and incontinence. At the time of examination, the individual had spastic gait typical to HSP, however she could walk without aid. Muscle strength was 4/5 in the lower limbs, and tendon reflexes were brisk in the four limbs with bilateral Babinski sign. There was no muscle wasting, there was no sensory deficit nor were there cerebellar or extrapyramidal signs. Motor coordination and cranial nerves examinations were normal. Eye movement and fundus examinations were normal. She had moderate bilateral pes valgus with hallux valgus. Electroneuromyography (ENMG) examination was normal. The individual also suffered from mild dysarthria.

## Family B.

### Individual IV-1

Individual IV-1 presented with onset of spastic paraplegia at the age of 35. He experienced lower limbs weakness that predominated on the left side and he also complained of dysarthria. No balance problems were reported. He was examined at the age of 47, and according to the individual he could walk more than 5000 meters, but had difficulties in running and going down the stairs. At the time of examination, Individual IV-1 had spastic gait, paralytic dysarthria with akinetic face, proximal reduced strength in lower limbs (4/5) and brisk tendon reflexes with bilateral

Babinski sign. There was no muscle wasting. He had bilateral and distal superficial hypoesthesia in both upper and lower limbs and reduced vibration sensation in lower limbs. The upper limb coordination and cranial nerves examination were normal. Eye movement and fundus examination were normal. He had no skeletal deformities. The ENMG examination showed a moderate sensory axonal neuropathy predominating in the lower limbs, sympathetic skin reflex was normal in upper limbs and abolished in lower limbs (Table S1).

**Individual IV-2**

Individual IV-2 presented with onset of spastic paraplegia at the age of 36 years with lower limbs weakness and ataxic gait. She was examined at the age of 44, and at the time of examination she needed cane support for walking, that she started using at the age of 40. At examination, the individual had reduced strength in lower limbs (4/5), without muscle wasting, and with brisk tendon reflexes in all limbs with bilateral Babinski sign. She had no sensory deficit, however she had moderate upper limbs dysmetria, as well as dysarthria and moderate facial hypokinesia. The cranial nerves examination was normal, with normal eye movement and fundus examination. Cognition was normal and there were no skeletal deformities with the exception of pes cavus. Her ENMG examination showed a moderate sensory axonal neuropathy predominating in the lower limbs, sympathetic skin reflex was normal in upper limbs and abolished in lower limbs (Table S1).

**Individual IV-4**

Individual IV-4 presented with onset of spastic paraplegia at the age of 22 years, with lower limbs stiffness at walking that progressed to spastic gait and weakness. He was examined at the age of

42 years old. At the time of the examination, he had spastic gait, however he reported that he could walk 1000 meters unaided. The lower limbs strength was 4/5 in proximal muscles and 5/5 in distal muscles, without muscle wasting. Tendon reflexes were brisk in all limbs with bilateral Babinski sign. He had no sensory deficit, and motor coordination and cranial nerve examinations were all normal. He had dysarthria and a subtle bilateral pes varus. Spinal cord and cerebral MRI were normal. Eye movement and fundus examinations were normal.

Blood tests were performed with the following results: normal sedimentation rate, complete blood count identified a moderate leukopenia (3900/$mm^3$), normal serum electrolytes and hepatic tests (bilirubin, transaminases, gamma-GT), moderate hyperlipidemia (Cholesterol - 2.73 g/l, triglycerides - 2.14 g/l), normal vitamin B12, B9 and vitamin E levels, moderately reduced vitamin B1 level (86 nmol/l), normal long chain fatty acids and phytanic acid levels. Immunoelectrophoresis of proteins and ponderal levels of immunoglobulins were normal.

**Individual IV-5**

Individual IV-5 presented with onset of spastic paraplegia at the age of 39 years. He was examined one year later at the age of 40. At the time of examination the individual had clear spastic gait with ataxia, however he could walk without aid. He had moderate dysarthria, normal strength in all muscles, and brisk tendon reflexes in all limbs. There was no muscle wasting in lower limbs. He had normal plantar cutaneous reflexes and normal sensory examination. He had a discrete upper limbs dysmetria and bilateral nystagmus. Eye movement and fundus examinations were normal. He had no skeletal deformities.

**Individual IV-9**

Individual IV-9 presented with onset of spastic paraplegia at the age of 24 with lower limbs stiffness when walking. At the time of examination, she was 30 years old. She had moderate lower limbs spasticity without any motor or sensory deficit, without muscle wasting. Tendon reflexes were brisk in all limbs with bilateral Babinski sign. There was no cerebellar or extrapyramidal signs. Eye movement and fundus examinations were normal. She had moderate bilateral pes cavus. The ENMG examination was normal but sympathetic skin reflex was normal in upper limbs and abolished in lower limbs (Table S1).

**Family C**

**Individual IV-7**

Individual IV-7 presented with onset of spastic paraplegia at the age of 33, with spastic gait and discoordination. His disease was slowly progressive, with little follow up. He was examined at the age of 35, and noted to have spastic gate, discoordination, bilateral Babinski sign, and ankle clonus. Cranial nerves examination was normal, including eye movement and fundus examination. Reported results from MRI were described as mild atrophy of cervical spinal cord. Individual IV-7 was lost of further follow-up.

**Individual IV-13**

Individual IV-13 presented with initial symptoms of spastic paraplegia at the age of 19, with mild lower limbs discoordination and weakness. At the first neurological examination, at the age of 22 years, she had normal motor examination with the exception of bilateral weakness (4/5) of the iliopsoas muscles. There was no muscle wasting. Sensory examination was normal. The gait was waddling, and she could not perform heel walk, and was unable to rise from a crouched position. Funduscopic examination and cranial nerves examination including eye movements were normal. Ten months prior to the first examination, she had CSF examination, myelogram and head CT, all of which were within the normal limit except for a slightly prominent sulci observed on the CT. At the time of recruitment, she was 31 years old, and presented with lower limbs spasticity, ataxic gait, poor balance and frequent tripping. Reflexes of the upper limbs were brisk and the lower limbs were spastic, with positive bilateral Babinski sign. Strength was 4/5 in both legs, and sensation was normal in both upper and lower limbs. She complained on urinary urgency and frequency, with stress incontinence, which deteriorated in the 3 years prior to the exam, and she also had pes cavus.

**Supplemental figures and legends**

**Figure S1 - *clp-1*(RNAi) produces motor phenotypes and axonal degeneration in *C. elegans***

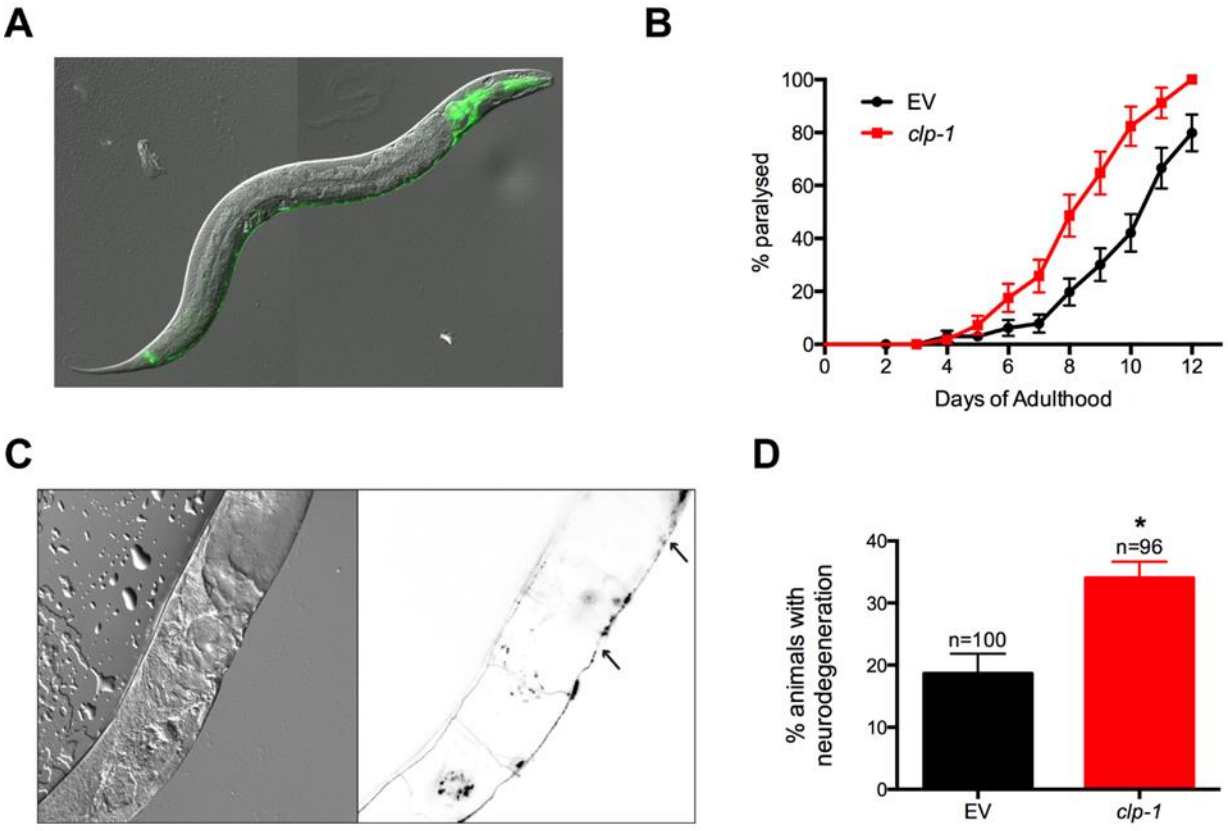


**Figure S1 legend**

***clp-1*(RNAi) produces motor phenotypes and axonal degeneration in *C. elegans***

The *C. elegans clp-1* encodes an orthologue of human calpain, and to investigate the contribution of *clp-1* to neuronal function, RNAi was used to knockdown the expression of endogenous *clp-1* in *C. elegans*. The *C. elegans strains* - XE137518 wpIs36 [unc-47p::mCherry] I; wpSi1 [unc-47p::rde-1::SL2::sid-1 + Cbr-unc-119(+)] II; eri-1(mg366) IV; rde-1(ne219) V; lin-15B(n744) X] were used for RNA interference (RNAi) assays. GABAergic neurons were visualized through and RNAi sensitivity only in GABAergic motor neurons was conveyed via wpSi1. Visualization of clp-1 expression was done using the transgenic GFP reporter strain BC1465819 dpy-5(e907) I;

sEx14658 [rCes C06G4.2b::GFP + pCeh361]. *RNAi procedures* - (RNAi)-treated strains were fed E. coli (HT115) containing an empty vector (EV) or clp-1(RNAi). RNAi clones were from the ORFeome RNAi library (Open Biosystems). RNAi experiments were performed at 20°C. Worms were grown on Nematode Growth Media enriched with 1 mM isopropyl-ß-D-thiogalactopyranoside. RNAi neurodegeneration tests were performed using the strain XE1375. Eggs were placed on plates with RNAi until day 5 of adulthood. Worms were transferred on fresh plates every 2 days. *Neurodegeneration assays* - For scoring of neuronal processes for gaps or breakage, XE1375 transgenic animals were selected at day 5 of adulthood for visualization of motor neuron processes in vivo. Animals were immobilized in 60% glycerol and mounted on slides with 2% agarose pads. mCherry was visualized at 585 nm using a Zeiss Axio Imager M2 microscope, using the Zen Pro 2012 software. Approximately 100 worms were scored per condition and each experiment was performed in triplicates. The mean and standard error of the mean were calculated for each trial and 2-tailed t tests were used for statistical analysis. Prism 5 (GraphPad Software) was used for all statistical analyses.

**A.** *clp-1*::GFP reporter shows expression in the pharynx, nerve ring, and along the ventral nerve cord. **B.** RNAi knockdown of the expression of endogenous *clp-1* in *C. elegans*. Worms treated with *clp-1*(RNAi) had motility defects, culminating in an age-dependent paralysis phenotype, which occurred at a higher frequency than control worms treated with empty vector (EV). RNAi *clp-1*(RNAi) (*clp-1*, n=62) enhances paralysis in a strain sensitized to RNAi only within the nervous system compared to empty vector (EV) controls (EV, n=72). Error bars represent SEM, ***P<0.001, log-rank (Mantel-Cox)-test. **C.** Visualization of neurodegeneration observed as gaps or breaks along neuronal processes (arrows) in a worm (*left*, differential interference contrast, *right*, inverted image from mCherry-fluorescence) in the nervous system exposed to *clp-1*(RNAi).

*clp-1* (RNAi) treatment resulted in degeneration, observed as gaps or breaks along axonal processes and this occurred at a greater rate than compared to EV RNAi control worms **D.** Quantification of neurodegeneration in worms treated with EV (n=100) or *clp-1*(RNAi) (n=96) during development and examined at day 5 of adulthood. *P<0.05, unpaired t-test. Error bars represent SEM. Overall, these data suggest that *clp-1* protects the nervous system against dysfunction and degeneration.

**Figure S2 - Pan neuronal expression of *calpain B* RNAi leads to defects in negative geotaxis in *Drosophila*.**

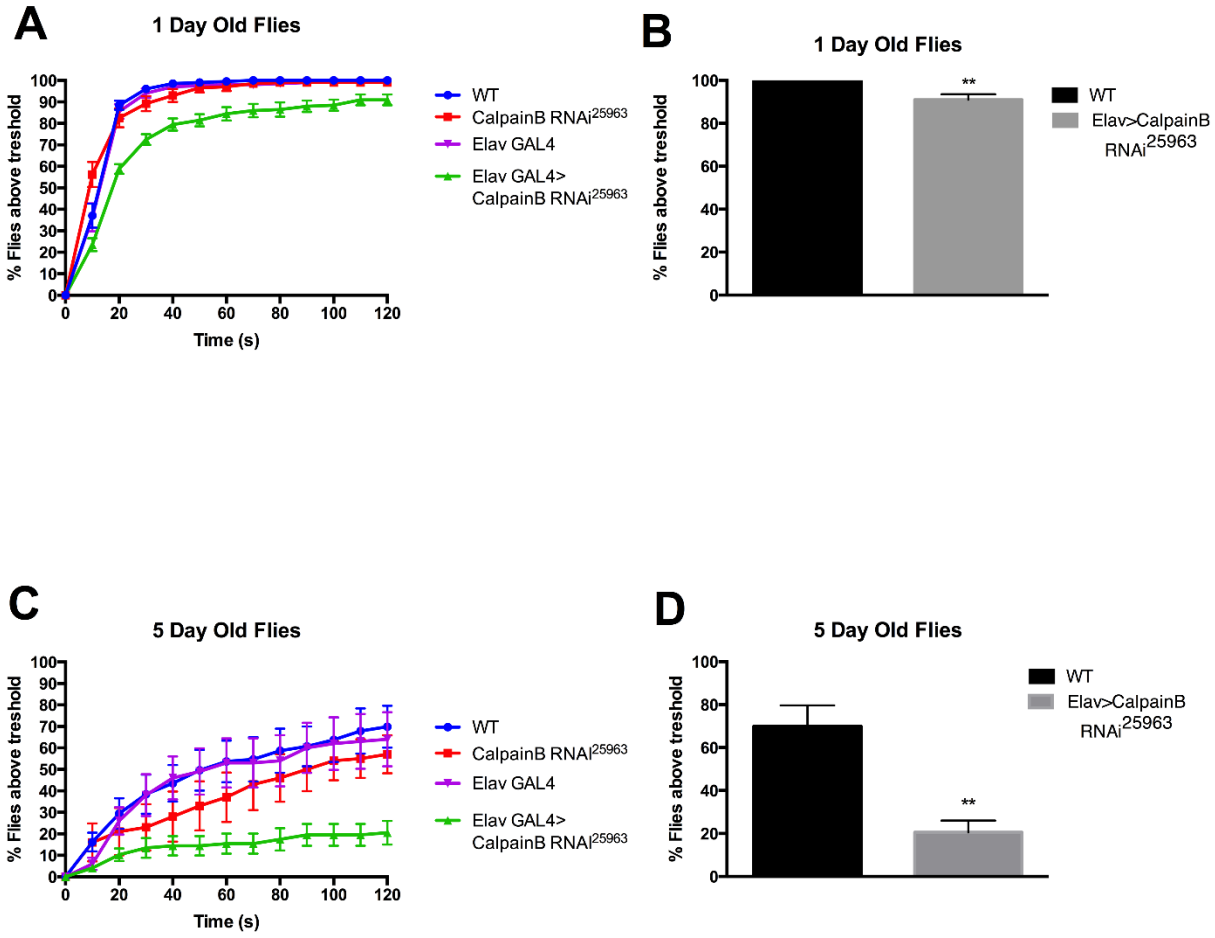


**Figure S2 legend**

*Drosophila* contains 3 paralogues of *CAPN1*. *Calpain B* has the highest homology with 45% blast identity versus 40% for *calpain A* and 28% for *calpain C* (Geneseer). Transgenic Drosophila containing the RNAi construct 25963 against Calpain B were obtained from the Vienna Drosophila Resource Center (VDRC). Pan-neuronal expression of the RNAi transgene was obtained by crossing the RNAi stocks to Elav-GAL4 homozygous flies. The flies were raised at 25°C. One day-old or 5 day-old flies were used for the climbing assay. Briefly, groups of 20 homogenous flies are tested at the time for their ability to climb in a glass cylinder above the 190mL line of a 250mL cylinder. The flies were filmed and then the percentage of flies that climbed above the

target line was plotted every 10 seconds, and results were plotted using Prism 5 (GraphPad Software). SigmaPlot 11.0 integrated with SigmaStat 3.1 was used to assess data groupings for significance. Statistical analyses used one-way ANOVA and Chi-square.

**A.** *Drosophila* transgenic for both the pan-neuronal driver ElavGAL4 and the responder UAS-calpain B RNAi present significant defect in their ability to climb above a reference target line when compared to the appropriate genetic controls (Elav GAL4 or UAS CalpainB RNAi. **B.** Climbing ability at 120 second for WT and Elav>CalpainB RNAi 25963 is significantly different (N=10, $p$=0.0064 t-test). **C.** Similarly, flies aged for 5 days show a more severe defect in climbing when compared to the same genetic controls. **D.** This defect is significant (N=5, $p$=0.0063 t-test).

**Figure S3 - Pan neuronal expression of calpain B RNAi leads to defects in neuromuscular junction neurons.**

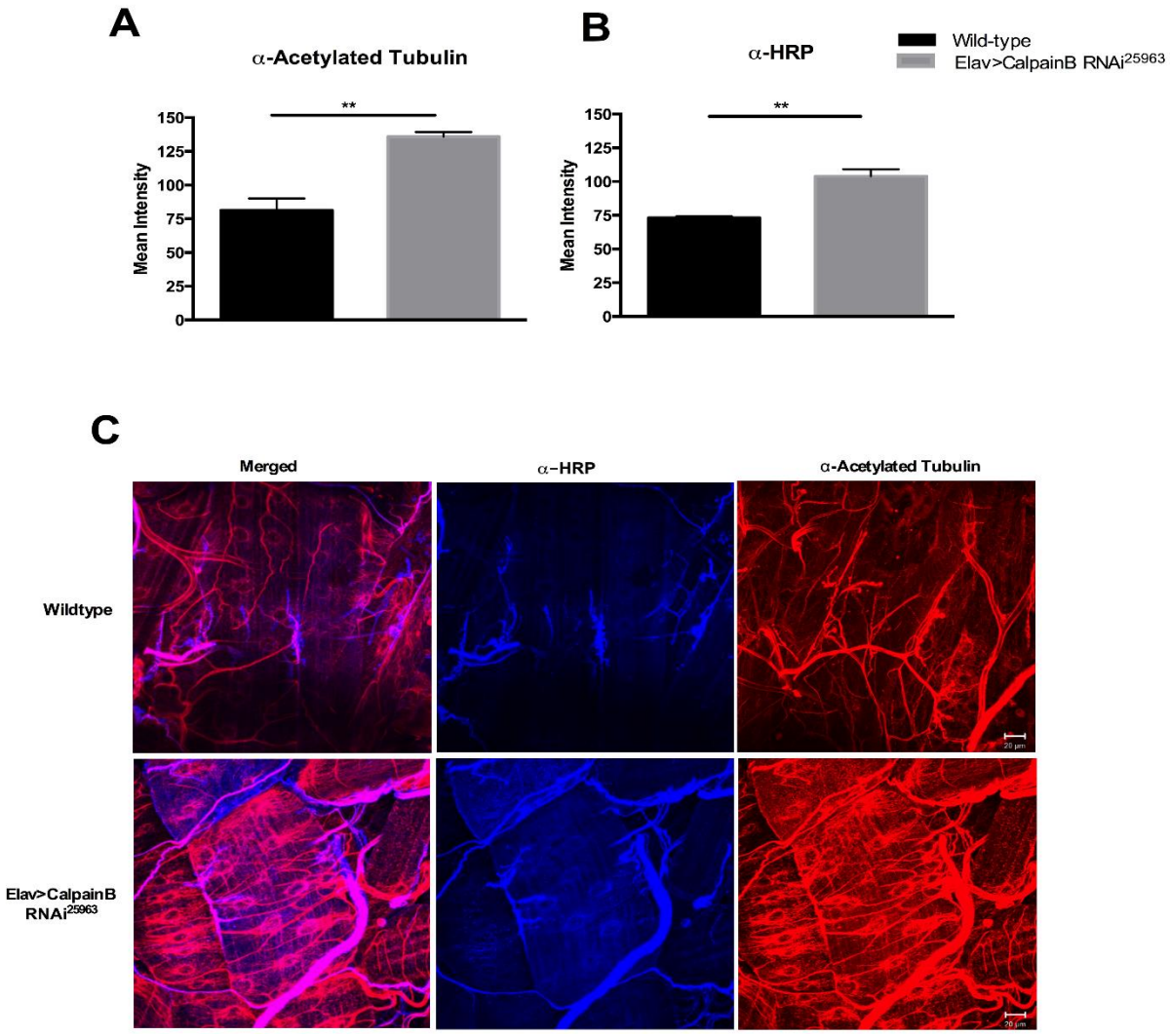


**Figure S3 legend**

Defects in axons were observed in transgenic flies expressing calpain B with the pan-neuronal driver Elav. Axons appeared of larger diameter and with increased level of acetylated tubulin. Increased acetylated tubulin is associated with hyperstabilization of microtubules and has been associated with *SPAST* mutations previously. Drosophila confocal imaging of the 3rd instar

neuromuscular junction was performed on third instar larvae. Antibodies against acetylated tubulin (Sigma T7451-200UL) and HRP (ThermoFisher PA1-26409) were utilized at a concentration of 1:1000. JacksonImmuno secondary antibodies Cy3 anti-mouse (115-165-003) and Cy5 anti-rabbit (JacksonIummuno 711-175-152) were purchased from Cedarlane and utilized at a concentration of 1:200.

Confocal imaging was performed using Zeiss LSM 700. Graph were made using data from mean intensity of the region of interest with Prism 5 (GraphPad Software). Image analysis was completed using ImageJ.

**A.** We observed a significant increase in the level of acetylated tubulin in the axons and muscles of the neuromuscular junction of larva expressing pan neuronally Calpain B RNAi. (N=3, P=0.0045, t-test). **B.** In addition, we observed that axons were larger on HRP immunohistochemistry suggesting larger fibers (N=3, P= 0.0039, t-test) **C.** Representative immunohistochemistry for the wild-type and pan-neuronal expressing Calpain RNAi larva. Interestingly, the acetylated tubulin were elevated and covered the entire diameter of large fibers compared to controls.

**Figure S4 - Clusters of acetylated tubulin are present in capn1a morphants zebrafish**

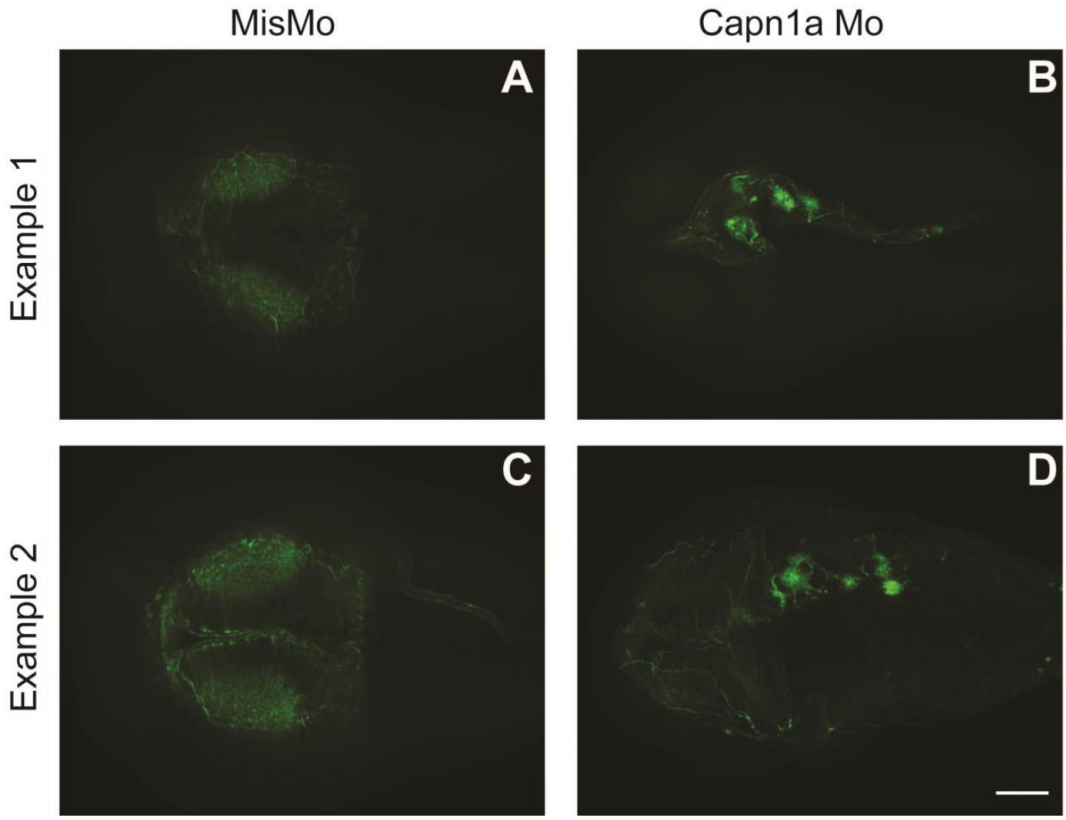


**Figure S4 legend**

Single slice images of acetylated tubulin staining in the brain of MisMo (**A, C**) and *capn1a* Mo (**B, D**) injected embryos. Images from 2 different embryos are shown for each condition, in order to show the variable clusters of acetylated tubulin observed in capn 1a morphants (**B, D**). Slices from the approximate same region of the brain are shown for the mismatch morphants (**A, C**). Scale bar is 60 μm.

**Figure S5. *Capn1a* morpholino induces morphological defects and abnormal development in *Danio rerio***

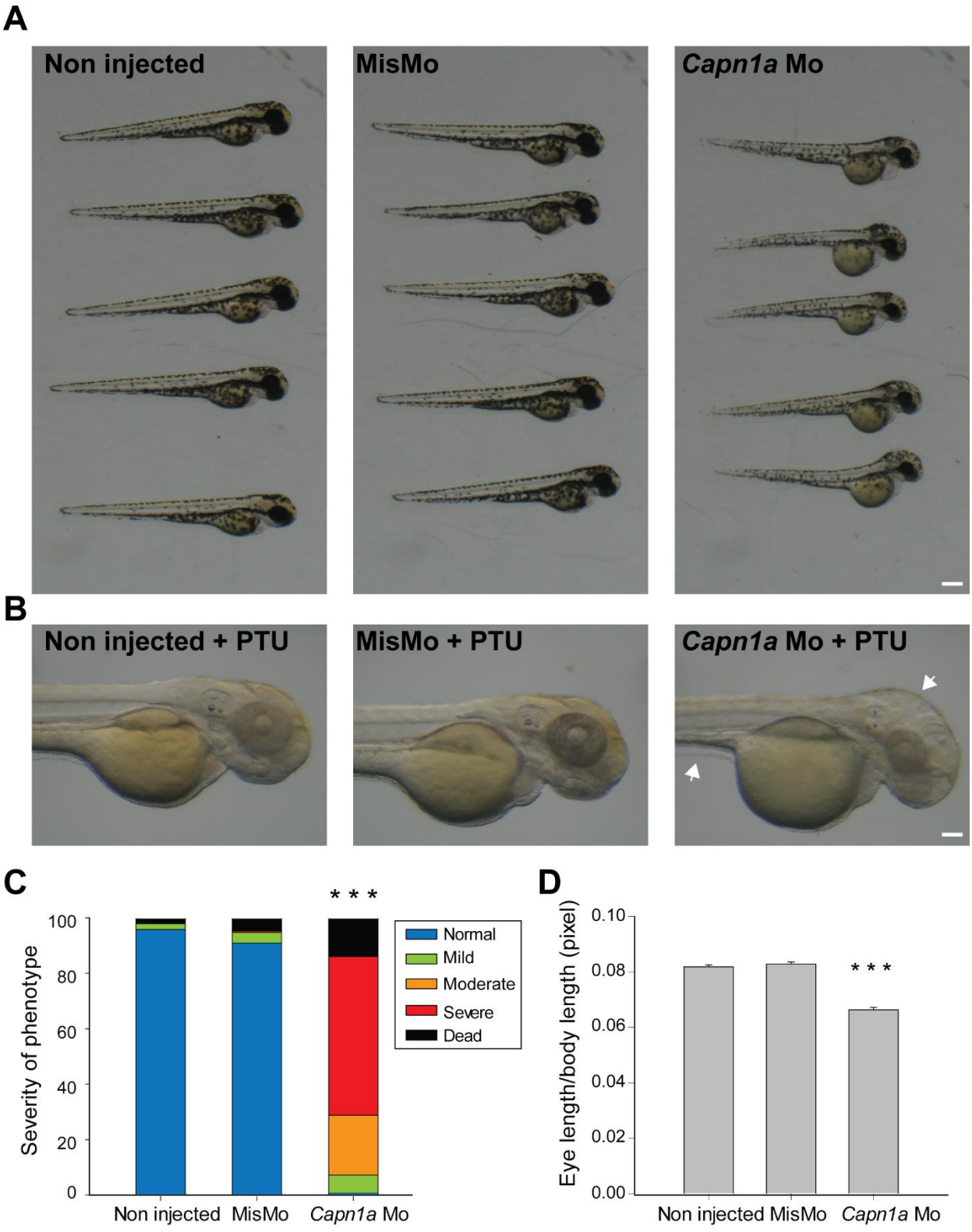

**Figure S5 legend**

Knockdown of zebrafish calpain1a and calpain 1b was achieved using morpholino oligonucleotides targeting the translation initiation site (*capn1a* Mo 5'-GAGATCCCGCCGTATGAGAACATGC-3'; *capn1b* Mo 5'-TCGACACACCTCCAATTGAAAACAT-3' Gene Tools, LLC). As an injection control, a mismatched *capn1a* morpholino with a five nucleotides substitution was used (MisMo 5'-GAcATCCaGCCcTATGAcAACATcC-3'). The morpholinos were diluted in deionized water with 0.05% Fast Green vital dye (Sigma) and 5 ng per embryo was pulse-injected into 1-4 cell stage embryos using a Picospritzer III pressure ejector. For this study, either AB-Tu wild-type or Islet1:GFP transgenic embryos were used. Embryos were kept until 5 days post-fertilization and the phenotype was quantified as follows: normal - no abnormal features or developmental delay; mild - absence of swim bladder; moderate - absence of swim bladder and presence of inflated pericardium; severe - absence of swim bladder, severely inflated pericardium with fluid accumulation around the yolk sac and extension. Eye phenotype assessment was performed using ImageJ 1.43m (NIH); the eye length was measured in the longitudinal plan, and divided by the length of the body, measured from the tip of the tail, until the frontal-most part of the head. Six hours post-fertilization embryos were treated with 0.2mM 1-phenyl 2-thiourea (PTU) until imaged, in order to prevent pigmentation from appearing. Two days post fertilization (dpf) embryos were anesthetized in 0.04% tricaine (Sigma) and mounted in 3% methylcellulose on a depression slide. The hindbrain of these embryos was visualized with a 10× water-immersion lens. Acetylated tubulin staining was performed as previously published. Briefly, 2 dpf embryos previously treated with PTU were fixed in Dent's fixative (80% methanol, 20% DMSO) overnight at 4 °C and washed 3X 10 minutes in 1% PBST. Embryos were blocked for one hour at room temperature in PBST

with 2% BSA and 2% normal goat serum, followed by an overnight incubation at 4°C with anti-acetylated tubulin monoclonal antibody (Sigma) in block (1:500). The next day, the embryos were washed 3X 10 minutes in PBST, then blocked for 1 hour, followed by a 4 hours incubation with a goat anti-mouse secondary antibody conjugated with Alex Fluor 488 (1:1,000). Embryos were then washed in PBST overnight, cleared in 80% glycerol and deyolked before being mounted either dorsal up, or on the side and imaged with a 10X air objective. Embryos were imaged with a Quorum Technologies spinning disk confocal microscope with a CSU10B (Yokogawa) spinning head mounted on an Olympus BX61W1 fluorescence microscope and connected to a Hamamatsu ORCA-ER camera and acquired using Volocity software (Improvision). The images were then processed using ImageJ 1.43m (NIH). Z-projections of confocal images are shown, except when otherwise specified.

**A.** Morphological features of 2 days post fertilization (dpf) embryos either not injected, injected with a mismatch morpholino (MisMo), or with a morpholino against *calpain 1a* (*Capn1a* Mo). Five representative embryos are shown for each condition. Scale bar is 250 μm. **B.** Non injected, MisMo injected and capn1a Mo injected embryos were treated with 1-phenyl 2-thiourea (PTU) to prevent pigmentation from developing. Arrows indicate defects in the head (hydrocephalus) and yolk sac extension. Scale bar is 50 μm. **C.** Quantification of severity of phenotype displayed at 5 dpf by non-injected (n=189), MisMo injected (n=209) and *capn1a* Mo (n=236) larvae. ***$p<0.001$, chi-square test. **C.** Ratio of the eye longitudinal length with the body length of 2 dpf non injected (0.0818, n=91), MisMo injected (0.0829, n=60) and *capn1a* Mo (0.0663, n=79) embryos. ***$p<0.001$, one-way ANOVA. Error bars represent standard error.

**Figure S6 - Western-blot analysis of calpain 1 expression levels in zebrafish**

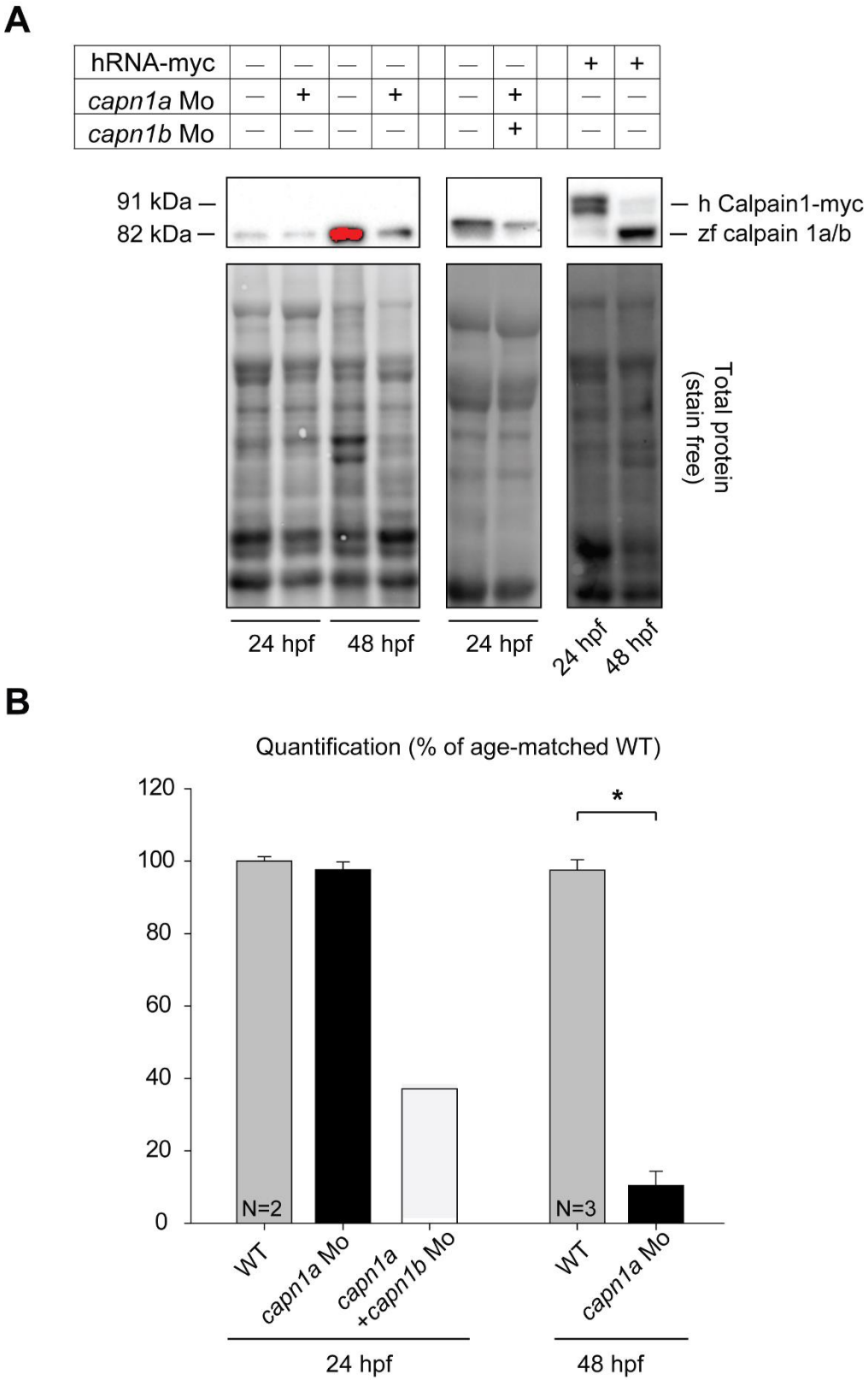

**Figure S6 legend**

About 30 embryos at 24 and 48 hours post-fertilization were lysed in ice-cold RIPA buffer (150 mM NaCl, 50 mM Tris pH 7.5, 1 % Triton X-100, 0.1 % SDS, 1 % Na deoxycholate, 0.1 % protease inhibitor), maintained on ice and homogenized with a hand-held pestle. The lysates were centrifuged for 10 minutes at 10,000 rpm at 4°C and the supernatant was collected. Protein concentration was established using Bio-Rad DC Protein Assay and 60 µg of proteins were loaded in 2X Lämmli buffer after boiling the samples for 5 minutes at 95°C. TGX Stain-Free FastCast acrylamide Kit (Bio-Rad) was used to make 10% Tris-glycine. After electrophoresis, the gels were activated by exposure to UV for one minute, and transferred to either regular or low-fluorescence PVDF membrane (Bio-Rad). After transfer, total proteins on membranes were detected by UV. Membranes were then blocked for one hour using 5 % fat free milk in PBST. The primary antibody (Calpain 1, 1:1000, Novus Biological NB120-3589) was incubated overnight at 4°C in 5 % fat free milk in PBST. After washing 3x 5 minutes in PBST, the membrane was incubated with an anti-mouse IgG, HRP conjugated (1:5000, Jackson Immuno) in 5 % fat free milk in PBST for one hour at room temperature, and then washed 3x 5 minutes. Membranes were exposed to Clarity enhanced chemiluminescence (ECL, Bio-Rad) for 5 minutes at room temperature and visualized using a ChemiDoc MP (Bio-Rad). Detection and quantification of band intensities was conducted using Image Lab 5.2 software (Bio-Rad). Bands were normalized to total protein by dividing the intensity of the band by the intensity of the total proteins from the same samples on the same blot, and the ratio was expressed as percentage of the age-matched wild-type control. Student's t-test was used to compare samples with their age-matched control. A value of $p < 0.05$ was considered statistically significant. **A.** Western blot analysis of calpain 1 in zebrafish at 24 hours post-fertilization (hpf) and 48 hpf without or with capn1a Mo knock down (first panel, the 48 hpf wild-type condition is saturated on purpose. This exposure time is not used for quantification); without

or with a double knock down of capn1a and capn1b (second panel); and following injection of 500 pg of human CAPN1 mRNA with 6x myc-tags, at 24 and 48 hpf (third panel, hRNA-myc). Total protein visualized by the stain-free technology is shown in the lower panel. **B.** Quantification of the western blots shown in A. The results are expressed as mean +/- SEM, * $p<0.05$. h: human; zf: zebrafish; hpf: hours post-fertilization; WT: wild-type.

**Supplemental tables**

**Table S1 – primers used for amplification and sequencing of *CAPN1* mutations**

| Variant | Forward | Reverse | Tm (c) | Length (bp) |
|---|---|---|---|---|
| p.Pro136Argfs*40 | AACCCCAGATTCTCCCTAGC | GCAGGTATTGTGGGTCATCC | 61 | 273 |
| c.1605+5G>A | CTGGAGTCTGGGTCTGGG | ACTCAGGGGACAGGACACC | 61 | 527 |
| p.Gln527* | CTGGAGTCTGGGTCTGGG | ACTCAGGGGACAGGACACC | 61 | 527 |
| p.Arg295Pro | AAGAGAATTGAATTGCTTGAACC | CGAGCAGAAATGTCGGG | 61 | 316 |

c, Celsius; bp, base-pares

**Table S2 – Genetic data on exome sequencing results**

| Family | Family A | Family B | Family C |
|---|---|---|---|
| **Number of individuals sequenced** | 3 | 4 | 2 |
| **Average coverage** | 133X | 130X | 121X |
| **All variants** | 215843 | 250171 | 168177 |
| **Coding/splicing** [a] | 37430 | 39414 | 28903 |
| **NS/SS/Indels** [b] | 16637 | 5400 | 15161 |
| **MAF 1KG** [c] | 2425 | 1841 | 2275 |
| **MAF EVS** [d] | 538 | 465 | 1815 |
| **Absent from In-house database** | 158 | 276 | 377 |
| **Common to affected** | 27 | 25 | 133 |
| **Genes with homozygous/compound heterozygous mutations** | 2 | 1 | 3 |
| **Deleterious** [e] | 1 | 1 | 1 |

[a] Filtering out variants that are not in the coding sequences or in the 6 base-pairs before and after the exon.

[b] Filtering out synonymous variants and including only non-synonymous/stop (NS), splice site (SS) and insertions and deletions (Indels).

[c] Including variants that had minor allele frequency (MAF) < 0.005 in the 1000 genome project (1KG) database.

[d] Including variants that had minor allele frequency (MAF) < 0.005 in the exome variant server (EVS) database.

[e] Predicted to be deleterious and conserved by SIFT, PolyPhen 2, MutationTaster, PhyloP and GERP++.

**Table S3 - Nerve conduction study data**

| | Family B Individual IV-1 | Family B Individual IV-2 | Family B Individual IV-9 | Family A Individual V-2 | Normal limits |
|---|---|---|---|---|---|
| **Median nerve** | L | L | L | NA | |
| DML (ms) | 3,5 | 3,6 | 3,1 | | < 4 |
| CMAP amplitude (mV) | 9,4 | 9,1 | 9,6 | | >4,8 |
| MNCV m/s | 60 | 62 | 58 | | > 47 |
| FWL (ms) | 28,8 | 23,3 | 23,7 | | <33 |
| **Ulnar nerve** | R | R | R | NA | |
| DML (ms) | 3,1 | 2,4 | 2,8 | | <3,2 |
| CMAP amplitude (mV) | 8,1 | 11,5 | 11,2 | | >4,8 |
| MNCV m/s | 58 | 63 | 60 | | > 47 |
| FWL (ms) | 28,6 | 25 | 25,8 | | <33 |
| **Peroneal nerve** | L | L | R | R | |
| DML (ms) | 6,3 | 5,6 | 4,9 | 3,8 | <6,5 |
| CMAP amplitude (mV) | 2,5 | 2,8 | 6,9 | 1,9 | >2 |
| MNCV m/s | 43 | 49 | 50 | 48,5 | >40 |
| FWL (ms) | 52,7 | 47,7 | 46,9 | 40,6 | <52 |
| **Tibial nerve** | R | R | NA | NA | |
| DML (ms) | 5 | 3,6 | | | <6 |
| CMAP amplitude (mV) | 4,3 | 5,3 | | | >3,5 |
| MNCV m/s | 46 | 50 | | | >40 |
| FWL (ms) | 50,5 | 45,2 | | | <52 |
| **Median nerve** | R | L | L | NA | |
| SNAP amplitude (uV) | 26,3 | 31 | 30 | | >12 |
| SCV (m/s) | NA | 47 | 50 | | >40 |
| **Ulnar nerve** | R | R | R | NA | |
| SNAP amplitude (uV) | 11,8 | 12 | 16 | | >8 |
| SCV (m/s) | NA | 55 | NA | | >40 |
| **Sural nerve** | R L | R L | R L | R L | |
| SNAP amplitude (uV) | 5,6 3,8 | 5,3 5,4 | 26 26 | 16 21 | >10 |
| SCV (m/s) | 38 39 | 40 41 | 32 33 | 45 36 | >35 |
| **Upper limbs** | L | L R | L R | NA | |
| Latency (s) | 1,7 | 1,39 1,35 | 1,23 1,38 | | Positive |
| **Lower limbs** | L | L R | L R | NA | |
| Latency (s) | NO | NO NO | NO NO | | Positive |

DML: distal motor latency; CMAP: compound muscle action potential; MNCV: motor nerve conduction velocity; FWL: F wave latency; SNAP: sensory nerve action potential; SCV: sensory conduction velocity; NA: not available; NO: not obtained; R: right; L: left.